Hindawi
Advances in Materials Science and Engineering
Volume 2018, Article ID 3762451, 6 pages
https://doi.org/10.1155/2018/3762451

*Research Article*

# Ab Initio Study of Optoelectronic and Magnetic Properties of Ternary Chromium Chalcogenides

**Marc Ong, Mahmoud Hammouri, and Radi A. Jishi**

*Department of Physics and Astronomy, California State University, 5151 State University Drive, Los Angeles, CA 90032, USA*

Correspondence should be addressed to Radi A. Jishi; rjishi@calstatela.edu

Received 29 June 2018; Accepted 19 October 2018; Published 15 November 2018

Academic Editor: Marco Cannas



Using first-principles calculations, we investigate the magnetic order in the ground state of several ternary chromium chalcogenide compounds. Electronic band structure calculations indicate that these compounds are either metallic or semiconductors with relatively low bandgap energies. The large optical absorption coefficients, predicted by our calculations, suggest that some of these compounds may be useful as light harvesters in solar cells or as infrared detectors.

## 1. Introduction

Ternary compounds of the form $ABX_3$, where $A$ and $B$ are metal atoms and $X$ is a halogen or a chalcogen, are exciting candidates as semiconductors for photovoltaics and other applications. These materials are highly tunable due to the large variety of possible elements that can be included. In addition to tunability, their low cost, facile synthesis, and long carrier lifetimes have gained the attention of the research community [1–3]. In particular, perovskite solar cells made from lead halide materials ($A\mathrm{Pb}X_3$) have enjoyed rapid development, with measured power conversion efficiencies rivaling state-of-the-art silicon devices [4–7]. As a result, there is interest in commercial application of lead-halide perovskites for photovoltaics; however, concerns regarding the toxicity of lead and high instability in the presence of moisture have hindered these efforts [2]. Thus, it would be of great interest to find materials with better stability and nontoxic composition, while still keeping the attractive properties of these lead-halide compounds.

Recently, ternary metal chalcogenide materials have been proposed as alternatives to these lead-halide perovskites [8, 9]. Materials of the form $ABO_3$ have been extensively studied and have been shown to be resilient in the presence of moisture [8, 10]. Unfortunately, the energy difference between transition metal $d$ orbitals and the $2p$ orbitals of oxygen results in a large bandgap; in fact, $BiFeO_3$, with a bandgap of 2.7 eV, has the lowest bandgap among this class of materials [10]. Solid solutions have been reported with bandgaps between 1.1 and 3.8 eV [8]; however, these materials have high intrinsic disorder.

To lower the bandgap of these $ABO_3$ materials, substitution of oxygen with chalcogens such as sulfur or selenium has been recently explored. Although reports of synthesis of these ternary transition metal chalcogenides have been around for a long time [11], there are still few studies focusing on their optoelectronic properties. Theoretical studies have been reported on substitution of oxygen with sulfur [12, 13]. Additionally, experimental reactions of perovskite oxides with gaseous $H_2S$ or $CS_2$ [14], as well as solid-state reactions have been recently reported as methods of substituting oxygen with sulfur [15, 16]. It has been shown that transition metal chalcogenides are widely tunable, ranging from metallic to semiconducting with gaps exceeding 2 eV [9, 16]. Several materials are predicted to have bandgaps corresponding to theoretical photovoltaic power conversion efficiencies above 28 percent [9], and zirconium sulfide perovskites have been experimentally measured to have strong optical absorption and a bandgap suitable for photovoltaic applications [16].

One interesting subset of these ternary transition metal chalcogenides are those of the form $A\mathrm{Cr}X_3$, where $X$ = S, Se,

or Te. Because of the presence of chromium, these materials tend to exhibit magnetic properties and have recently seen a resurgence of interest [17, 18]. Several of these materials, such as $SbCrS_3$ [19], $SbCrSe_3$ [18–20], and $SiCrTe_3$ [21, 22], have been the subjects of recent experimental studies as magnetic materials with metallic or semiconducting behavior. However, many of these materials, including many of the lanthanide chromium sulfides, have not been thoroughly studied even though their syntheses have been reported a long time ago [11].

In this work, we present first-principles calculations on some chromium chalcogenides where experimentally determined crystal data are available, but electronic or magnetic properties have not been thoroughly investigated. Using total energy calculations, we determine the ground-state magnetic ordering at 0 K and then calculate optoelectronic properties to determine their usefulness in various applications.

With the exception of $PCrSe_3$ and $SiCrTe_3$, all the structures examined have the space group 62 (*Pnma*) and they adopt the $NH_4CdCl_3$ prototype structure. This structure contains dimers of $CrX_6$ ($X$ = S, Se, or Te) octahedra and ninefold coordination between the $A$ site and the chalcogen atoms. Unlike the perovskite structure, which contains corner-sharing octahedra [23, 24], the octahedra in this structure share edges, as shown in Figure 1.

The structure of $PCrSe_3$ is monoclinic with space group 12 ($C2/m$). This structure contains layers of a single P atom surrounded by six $CrSe_6$ octahedra in the *ab* plane, as pictured in Figure 2.

The structure of $SiCrTe_3$ is rhombohedral with space group 148 ($R\bar{3}$) and is shown in Figure 3. In this structure, edge-sharing $CrTe_6$ octahedra form layers on the *ab* plane, while the Si atoms have threefold coordination with the Te atoms.

## 2. Methods

To determine the ground-state magnetic ordering of the chromium chalcogenides, we used density functional theory (DFT) as implemented in the Vienna Ab Initio Simulation Package (VASP) [25–28] code, which uses the projector-augmented wave (PAW) pseudopotentials and a plane-wave basis set to expand the electronic wave function. The Perdew–Burke–Ernzerhof implementation of the generalized gradient approximation (PBE–GGA) was used to model the exchange-correlation effects [29, 30]. We performed spin-polarized calculations, where varying spin orderings were imposed on the chromium ions. A Hubbard on-site Coulomb term ($U$ = 4 eV) and Hund's exchange term ($J$ = 0.7 eV) for the chromium ions are included in the calculation. Experimentally determined crystal structures from the Inorganic Crystal Structure Database were used in our calculations, with the exception of $SiCrTe_3$, where the X-ray diffraction measurements at 292 K of Casto et al. were used [21]. The total energies of different magnetic orders were compared to determine the ground state.

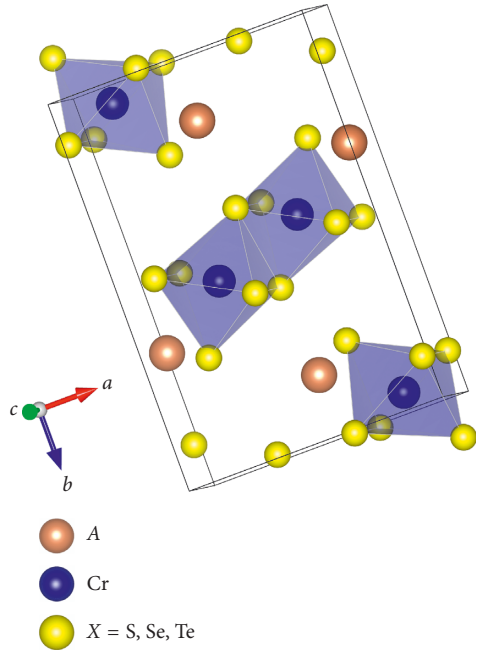


Figure 1: Visualization of the unit cell of the $NH_4CdCl_3$ prototype structure, which contains edge-sharing octahedra.

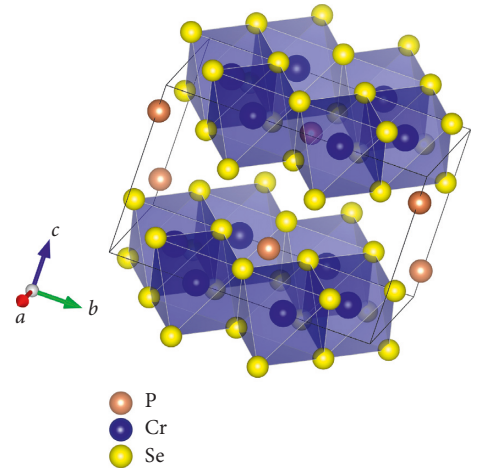


Figure 2: Visualization of the unit cell of $PCrSe_3$.

The electronic band structures, density of states, and optical properties were calculated using the full-potential, linearized, augmented plane wave (FP–LAPW) method, as implemented in the WIEN2k code [31]. Here, space is divided into an interior region of nonoverlapping muffin tin spheres centered on each atom and an exterior region comprising the interstitial space between these spheres. Within the spheres, the electronic wave function is treated as atomic like, with an expansion in spherical harmonics up to $\ell_{max} = 10$. Within the interstitial space, the wave function is expanded in plane waves, with a maximum wave vector of $k_{max}$. The maximum wave vector is determined by setting $R_{mt}k_{max} = 8$, where $R_{mt}$ is the radius of the smallest sphere. The charge density is Fourier expanded up to a maximum

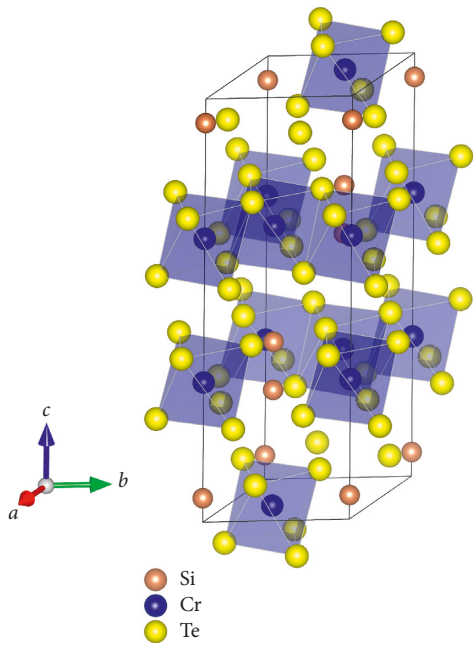


Figure 3: Visualization of the unit cell of $SiCrTe_3$.

wave vector of $14/a_0$, where $a_0$ is the Bohr radius. On-site Coulomb interaction was taken into account, using the same $U$ and $J$ values from the VASP total energy calculation. We performed self-consistent field calculation until energy convergence within $10^{-4}$ Ry and charge convergence within $10^{-3}$ $e$ were achieved. The calculations were spin polarized, and we used the magnetic order in the ground state which was determined in the VASP calculation.

The optical properties of the chromium chalcogenides were calculated using the wave functions obtained from the electronic calculation. Specifically, the imaginary part of the dielectric function $\varepsilon_2(\omega)$ was obtained using the following momentum matrix elements [32]:

$$\varepsilon_2(\omega) = \frac{V_{\text{cell}} e^2}{2\pi\hbar m^2 \omega^2} \int d^3k \sum_{nn'} \left|\langle \mathbf{k}n|\mathbf{p}|\mathbf{k}n'\rangle\right|^2 \times f(\mathbf{k}n)\left[1 - f(\mathbf{k}n')\right]\delta\left(E_{\mathbf{k}n} - E_{\mathbf{k}n'} - \hbar\omega\right), \quad (1)$$

where $\mathbf{p}$ is the momentum operator, $|\mathbf{k}n\rangle$ is a crystal wave function with energy eigenvalue $E_{\mathbf{k}n}$, $\hbar\omega$ is the photon energy, and $f$ is the Fermi-Dirac distribution function. A Kramers–Kronig transformation was used to obtain the real part of the dielectric function $\varepsilon_1(\omega)$, and the absorption coefficient $\alpha(\omega)$ was calculated as

$$\alpha(\omega) = \sqrt{2}\omega\left[\sqrt{\varepsilon_1(\omega)^2 + \varepsilon_2(\omega)^2} - \varepsilon_1(\omega)\right]^{1/2}. \quad (2)$$

## 3. Results and Discussion

The energies of different magnetic structures for the chromium chalcogenides studied are listed in Table 1. Here, $A$-type antiferromagnetism ($A$-AFM) denotes ferromagnetism within the $ac$ plane and antiferromagnetism between planes, $C$-type antiferromagnetism ($C$-AFM) denotes ferromagnetism between planes and antiferromagnetism within the plane, and $G$-type antiferromagnetism ($G$-AFM) denotes antiferromagnetism both within and between planes. Experimental results have shown that most of these materials, such as $SbCrS_3$ [19], $SbCrSe_3$ [18], and $SiCrTe_3$ [21], have magnetic order at low temperatures but are paramagnetic at room temperature. The predicted magnetic structure of $SbCrS_3$ [19], $SbCrSe_3$ [19], $LaCrS_3$ [33], $SbCrS_3$ [33], and $SiCrTe_3$ [21] agree with experimental measurements. For $LaCrSe_3$ and $CeCrSe_3$, there seems to be ambiguity as to whether the structure is antiferromagnetic or weakly ferromagnetic [34], and this is reflected in our calculations by the fact that the energy differences between ferromagnetic and antiferromagnetic states are very small.

The bandgaps calculated using DFT + $U$ for the chalcogenides are given in Table 2 and compared with experimental results. These compounds range in character from metallic to semiconducting with small gaps, the largest of which is 1.29 eV. Due to the scarcity of experimental studies on these materials, information regarding the bandgaps of most materials is not available; however, we remark that the calculated bandgap values for $SbCrSe_3$ and $SiCrTe_3$ with our chosen values of $U$ and $J$ are in good agreement with experiment.

The calculated electronic band structure and density of states of the majority-spin carriers in $GaCrSe_3$ and $SbCrS_3$ are shown in Figures 4 and 5, respectively. These structures were chosen because their bandgaps are suitable for photovoltaic applications. For $GaCrSe_3$, we find a direct bandgap of 1.29 eV at Γ, while for $SbCrSe_3$, we find a direct bandgap of 1.47 eV at Γ and an indirect bandgap of 0.98 eV corresponding to the $\Gamma \longrightarrow T$ transition. In both of these structures, the density of states near both conduction band and valence band edges are primarily contributed by chromium $d$ orbitals and chalcogenide $p$ orbitals. In $GaCrS_3$, the narrowness of the bands gives rise to high density of states, reaching a maximum of around 20 states/eV above the conduction band. $SbCrSe_3$ has a slightly smaller density of states, with a maximum of around 15 states/eV above the conduction band.

In addition to the density of states, we also calculated the optical properties for $GaCrSe_3$ and $SbCrS_3$, as well as $CrSiTe_3$ and $SbCrSe_3$, which were found to be narrow-gap semiconductors. The absorption curves, shown in Figure 6, agree with the bandgap values calculated for these chalcogenides. From this figure, we see that they exhibit strong absorption ($> 10^5\ \text{cm}^{-1}$) in the infrared and visible regions, suggesting that these materials may be of interest for photovoltaic applications. These large values for the absorption coefficients are comparable to those measured in Zr-based chalcogenides [16]. Additionally, absorption coefficients larger than $10^5\ \text{cm}^{-1}$ are observed at significantly lower energies than that of pure silicon, which is the industry standard for photovoltaics. Silicon does not achieve such a value for the absorption coefficient until a photon energy of approximately 3 eV is reached [35]; on the contrary, we observe that $SbCrS_3$ and $GaCrSe_3$, with

Table 1: Calculated energies (in meV per formula unit) of different magnetic states of the chromium chalcogenides. The energy of the lowest state for each material is set to zero for ease of comparison. For $PCrSe_3$, $\alpha = \gamma = 90^\circ$ and $\beta = 107.71^\circ$. For $SiCrTe_3$, $\alpha = \beta = \gamma = 50.56^\circ$. For $SiCrTe_3$, each unit cell contains two Cr atoms; hence, there is only one possible antiferromagnetic state.

| Crystal | Space group | Lattice constants (Å) | *A*-AFM | *C*-AFM | *G*-AFM | FM |
|---|---|---|---|---|---|---|
| $PCrSe_3$ | 12 ($C2/m$) | $a = 6.15, b = 10.59, c = 6.69$ | 0 | 88.50 | 46.00 | 27.25 |
| $SbCrS_3$ | 62 ($Pnma$) | $a = 8.67, b = 3.62, c = 12.87$ | 24.07 | 3.50 | 15.20 | 0 |
| $SbCrSe_3$ | 62 ($Pnma$) | $a = 9.14, b = 3.78, c = 13.32$ | 41.83 | 2.42 | 27.95 | 0 |
| $LaCrS_3$ | 62 ($Pnma$) | $a = 7.87, b = 3.85, c = 13.84$ | 12.62 | 0 | 6.81 | 0.43 |
| $LaCrSe_3$ | 62 ($Pnma$) | $a = 8.11, b = 3.96, c = 13.79$ | 13.52 | 5.57 | 0 | 9.29 |
| $CeCrS_3$ | 62 ($Pnma$) | $a = 7.76, b = 3.79, c = 13.16$ | 0 | 14.93 | 34.51 | 13.27 |
| $CeCrSe_3$ | 62 ($Pnma$) | $a = 8.08, b = 3.95, c = 13.74$ | 12.97 | 2.20 | 2.87 | 0 |
| $GaCrSe_3$ | 62 ($Pnma$) | $a = 10.12, b = 3.73, c = 12.39$ | 14.66 | 1.05 | 13.64 | 0 |
| $SiCrTe_3$ | 148 ($R\bar{3}$) | $a = b = c = 8.00$ | 39.87 | — | — | 0 |

Table 2: Comparison of DFT + $U$ bandgaps with experimental results.

| Crystal | Calculated gap (eV) | Experimental gap (eV) |
|---|---|---|
| $PCrSe_3$ | 0 | — |
| $SbCrS_3$ | 0.98 | — |
| $SbCrSe_3$ | 0.63 | 0.6–0.7 [18] |
| $LaCrS_3$ | 0.20 | — |
| $LaCrSe_3$ | 0.07 | — |
| $CeCrS_3$ | 0 | — |
| $CeCrSe_3$ | 0 | — |
| $GaCrSe_3$ | 1.29 | — |
| $SiCrTe_3$ | 0.40 | 0.4 [21] |

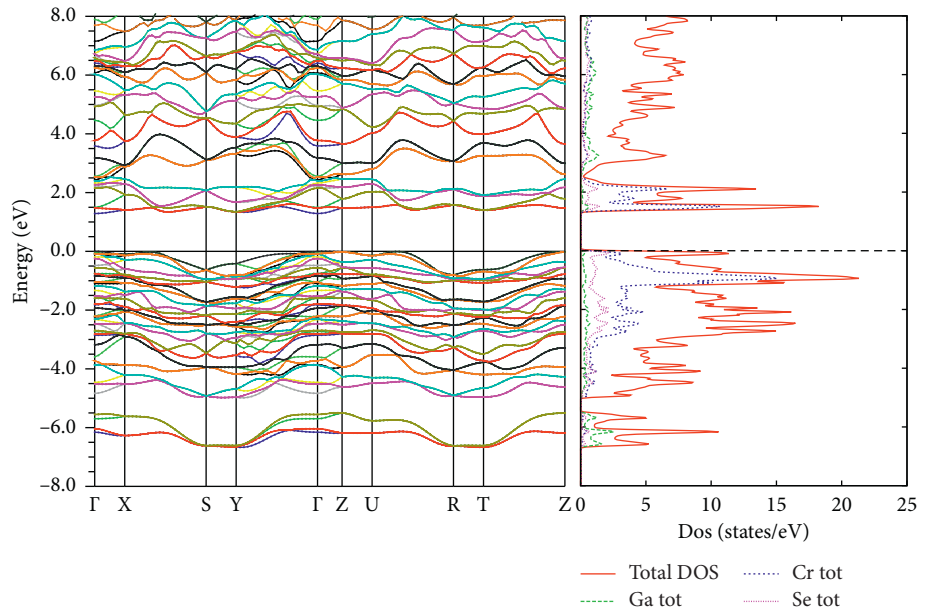


Figure 4: Calculated electronic band structure and density of states for $GaCrSe_3$.

comparable bandgaps to silicon, achieve this value at 1.5 eV and 2 eV, respectively. This would allow for better capture of light in the near-infrared and visible ranges. The narrow bandgap $SbCrSe_3$ and $SiCrTe_3$ may be useful for infrared detection applications, while $SbCrS_3$ and $GaCrSe_3$ may be possible candidates for use as light absorbers in photovoltaics.

## 4. Conclusion

In conclusion, we have carried out density functional theory calculations on various chromium chalcogenide materials. We have demonstrated that calculations within the DFT + $U$ scheme accurately predict the magnetic structure and energy gaps of this class of materials. We have identified two

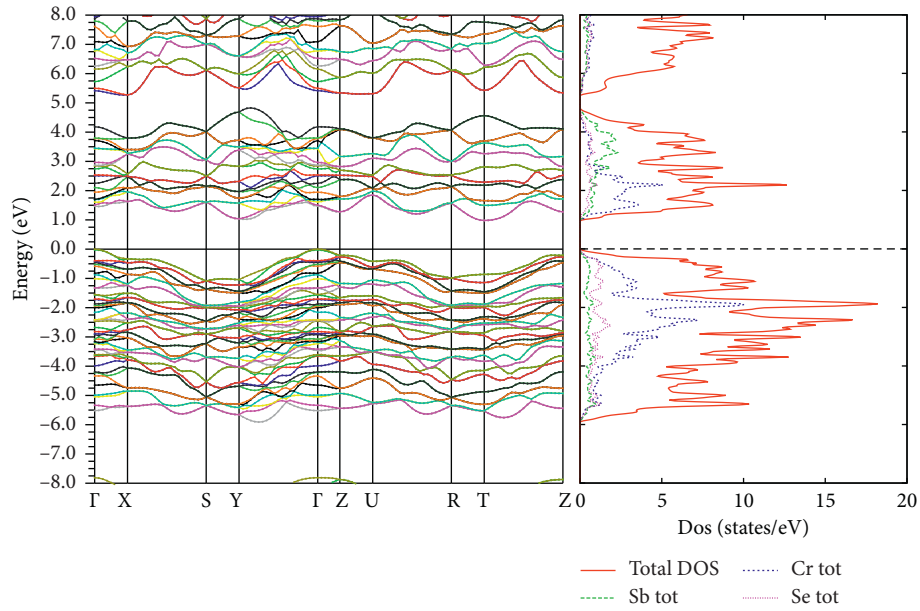


Figure 5: Calculated electronic band structure and density of states for $SbCrS_3$.

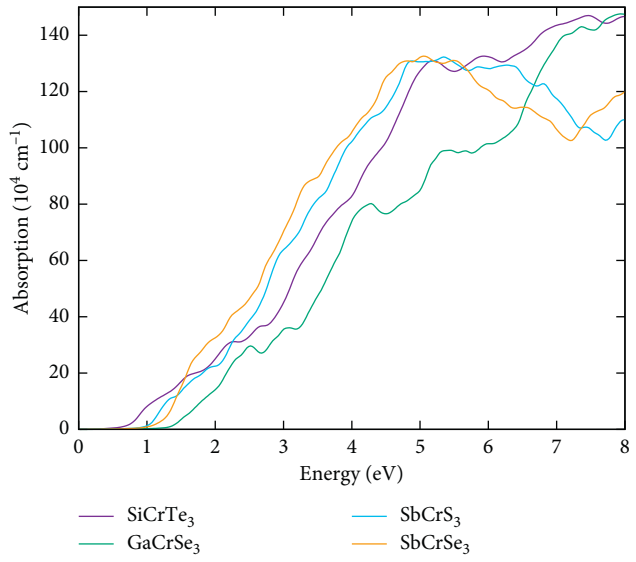


Figure 6: Calculated optical absorption spectra for semiconductor chromium chalcogenides.

materials, namely, $GaCrSe_3$ and $SbCrS_3$, whose bandgaps and strong optical absorption make them candidates for use in photovoltaics, as well as the narrow-gap semiconductors $SbCrSe_3$ and $SiCrTe_3$, which may be of interest for infrared detection applications.

## Data Availability

No supporting information is available.

## Conflicts of Interest

The authors declare no conflicts of interest.

## Acknowledgments

This work was supported by the National Science Foundation under grant HRD-15477723 and grant DMR-15235885.

## References

[1] S. D. Stranks, G. E. Eperon, G. Grancini et al., "Electron-hole diffusion lengths exceeding 1 micrometer in an organometal trihalide perovskite absorber," *Science*, vol. 342, no. 6156, pp. 341–344, 2013.

[2] M. Grätzel, "The light and shade of perovskite solar cells," *Nature Materials*, vol. 13, no. 9, pp. 838–842, 2014.

[3] N. J. Jeon, J. H. Noh, W. S. Yang et al., "Compositional engineering of perovskite materials for high-performance solar cells," *Nature*, vol. 517, no. 7535, pp. 476–480, 2015.

[4] Q. Chen, H. Zhou, Z. Hong et al., "Planar heterojunction perovskite solar sells via vapor-assisted solution process," *Journal of the American Chemical Society*, vol. 136, no. 2, pp. 622–625, 2014.

[5] H. J. Snaith, "Perovskites: the emergence of a new era for low-cost and high-efficiency solar cells," *Journal of Physical Chemistry Letters*, vol. 4, no. 21, pp. 3623–3630, 2013.

[6] H.-S. Kim, S. H. Im, and N.-G. Park, "Organolead halide perovskite: new horizons in solar cell research," *Journal of Physical Chemistry C*, vol. 118, no. 11, pp. 5615–5625, 2014.

[7] M. Saliba, T. Matsui, K. Domanski et al., "Incorporation of rubidium cations into perovskite solar cells improves photovoltaic performance," *Science*, vol. 354, no. 6309, pp. 206–209, 2016.

[8] I. Grinberg, D. V. West, M. Torres et al., "Perovskite oxides for visible-light-absorbing ferroelectric and photovoltaic materials," *Nature*, vol. 503, no. 7407, pp. 509–512, 2013.

[9] Y.-Y. Sun, M. L. Agiorgousis, P. Zhang, and S. Zhang, "Chalcogenide perovskites for photovoltaics," *Nano Letters*, vol. 15, no. 1, pp. 581–585, 2015.

[10] W. S. Choi, M. F. Chisholm, D. J. Singh, T. Choi, G. E. J. Jr., and H. N. Lee, "Wide bandgap tunability in complex transition metal oxides by site-specific substitution," *Nature Communications*, vol. 3, no. 1, p. 689, 2012.

[11] T. Takahashi, T. Oka, O. Yamada, and K. Ametani, "Synthesis and crystallographic properties of lanthanum transition metal sulfides La$MS_3$; $M$ = Cr, Mn, Fe, and Co," *Materials Research Bulletin*, vol. 6, no. 3, pp. 173–181, 1971.

[12] B. Kolb and A. M. Kolpak, "First-principles design and analysis of an efficient, pb-free ferroelectric photovoltaic absorber derived from $ZnSnO_3$," *Chemistry of Materials*, vol. 27, no. 17, pp. 5899–5906, 2015.

[13] R. A. Jishi and M. A. Lucas, "$ZnSnS_3$: structure prediction, ferroelectricity, and solar cell applications," *International Journal of Photoenergy*, vol. 2016, Article ID 6193502, 9 pages, 2016.

[14] S. Perera, H. Hui, C. Zhao et al., "Chalcogenide perovskites-an emerging class of ionic semiconductors," *Nano Energy*, vol. 22, pp. 129–135, 2016.

[15] W. Meng, B. Saparov, F. Hong, J. Wang, D. B. Mitzi, and Y. Yan, "Alloying and defect control within chalcogenide perovskites for optimized photovoltaic application," *Chemistry of Materials*, vol. 28, no. 3, pp. 821–829, 2016.

[16] S. Niu, H. Huyan, Y. Liu et al., "Bandgap control via structural and chemical tuning of transition metal perovskite chalcogenides," *Advanced Materials*, vol. 29, no. 9, article 1604733, 2016.

[17] A. Narayan, A. Bhutani, S. Rubeck, J. N. Eckstein, D. P. Shoemaker, and L. K. Wagner, "Computational and experimental investigation for new transition metal selenides and sulfides: the importance of experimental verification for stability," *Physical Review B*, vol. 94, no. 4, article 045105, 2016.

[18] T. Kong, K. Stolze, D. Ni, S. K. Kushwaha, and R. J. Cava, "Anisotropic magnetic properties of the ferromagnetic semiconductor $CrSbSe_3$," *Physical Review Materials*, vol. 2, no. 1, article 014410, 2018.

[19] V. Volkov, G. V. Tendeloo, J. V. Landuyt et al., "Hrem image analysis up to structure determination of $SbCrSe_3$: a new 1D ferromagnet," *Journal of Solid State Chemistry*, vol. 132, no. 2, pp. 257–266, 1997.

[20] D. Yang, W. Yao, Y. Yan et al., "Intrinsically low thermal conductivity from a quasi-one-dimensional crystal structure and enhanced electrical conductivity network via Pb doping in $SbCrSe_3$," *NPG Asia Materials*, vol. 9, no. 6, p. e387, 2017.

[21] L. D. Casto, A. J. Clune, M. O. Yokosuk et al., "Strong spin-lattice coupling in $CrSiTe_3$," *APL Mater*, vol. 3, no. 4, article 041515, 2015.

[22] M.-W. Lin, H. L. Zhuang, J. Yan et al., "Ultrathin nanosheets of $CrSiTe_3$: a semiconducting two-dimensional ferromagnetic material," *Journal of Materials Chemistry C*, vol. 4, no. 2, pp. 315–322, 2016.

[23] M. W. Lufaso and P. M. Woodward, "Prediction of the crystal structures of perovskites using the software program," *Acta Crystallographica Section B Structural Science*, vol. 57, no. 6, pp. 725–738, 2001.

[24] H. Zhang, N. Li, K. Li, and D. Xue, "Structural stability and formability of $ABO_3$-type perovskite compounds," *Acta Crystallographica Section B Structural Science*, vol. 63, no. 6, pp. 812–818, 2007.

[25] G. Kresse and J. Hafner, "Ab initio molecular dynamics for liquid metals," *Physical Review B*, vol. 47, no. 1, pp. 558–561, 1993.

[26] G. Kresse and J. Hafner, "Ab initio molecular-dynamics simulation of the liquid-metal amorphous-semiconductor transition in germanium," *Physical Review B*, vol. 49, no. 20, pp. 14251–14269, 1994.

[27] G. Kresse and J. Furthmüller, "Efficiency of ab-initio total energy calculations for metals and semiconductors using a plane-wave basis set," *Computational Materials Science*, vol. 6, no. 1, pp. 15–50, 1996.

[28] G. Kresse and J. Furthmüller, "Efficient iterative schemes for ab initio total-energy calculations using a plane-wave basis set," *Physical Review B*, vol. 54, pp. 11169–11186, 1996.

[29] J. P. Perdew, K. Burke, and M. Ernzerhof, "Generalized gradient approximation made simple," *Physical Review Letters*, vol. 77, no. 18, pp. 3865–3868, 1996.

[30] J. P. Perdew, K. Burke, and M. Ernzerhof, "Errata: generalized gradient approximation made simple," *Physical Review Letters*, vol. 78, no. 7, p. 1396, 1997.

[31] P. Blaha, K. Schwarz, G. K. H. Madsen, D. Kvasnicka, and J. Luitz, *WIEN2k, An Augmented Plane Wave + Local Orbitals Program for Calculating Crystal Properties*, Karlheinz Schwarz-echnische Universität Wien, Austria, 2001, ISBN: 3-9501031-1-2.

[32] S. Saha, T. Sinha, and A. Mookerjee, "Electronic structure, chemical bonding, and optical properties of paraelectric $BaTiO_3$," *Physical Review B*, vol. 62, no. 13, pp. 8828–8834, 2000.

[33] S. Kikkawa, Y. Fujii, Y. Miyamoto et al., "High-pressure synthesis of La$MS_3$ ($M$ = Ti, V, Cr)," *Journal of Solid State Chemistry*, vol. 139, no. 2, pp. 233–237, 1998.

[34] O. Gorochov and H. McKinzie, "The magnetic and electrical properties of $LnCrSe_3$ (Ln = La, Ce, Pr, Nd)," *Journal of Solid State Chemistry*, vol. 7, no. 4, pp. 400–407, 1973.

[35] W. Dash and R. Newman, "Intrinsic optical absorption in single-crystal germanium and silicon at 77 k and 300 k," *Phys. Rev.,* vol. 99, no. 4, pp. 1151–1155, 1955.